photonics

MDPI

Communication

Prediction of Power Fluctuations of Gaussian Beams After Transmission Through Turbulent Atmosphere

Zhihao Wan [1], Jiayi Zhu [1], Cheng Huang [1], Zhimin He [1], Jun Zeng [1], Fuchang Chen [1], Chaoqun Yu [1], Yan Li [1], Huanting Chen [1], Yongtao Zhang [1], Jixiong Pu [1,2,3] and Huichuan Lin [1,*]

[1] Key Laboratory of Light Field Manipulation and System Integration Applications in Fujian Province, College of Physics and Information Engineering, Minnan Normal University, Zhangzhou 363000, China; wzh2023@mnnu.edu.cn (Z.W.); zjy2022@mnnu.edu.cn (J.Z.); hc0223@mnnu.edu.cn (C.H.); hzm0191@mnnu.edu.cn (Z.H.); zj1838@mnnu.edu.cn (J.Z.); cfc1614@mnnu.edu.cn (F.C.); ycq1650@mnnu.edu.cn (C.Y.); ly1734@mnnu.edu.cn (Y.L.); cht1521@mnnu.edu.cn (H.C.); yongtaozhang@mnnu.edu.cn (Y.Z.); jixiong@hqu.edu.cn (J.P.)

[2] Fujian Provincial Key Laboratory of Light Propagation and Transformation, College of Information Science & Engineering, Huaqiao University, Xiamen 361021, China

[3] Dongguan Guangda Intelligent Technology Co., Ltd., Dongguan 523808, China

* Correspondence: lhc1810@mnnu.edu.cn; Tel.: +86-18876330655

Abstract: As laser beams propagate through free space, power fluctuation occurs due to atmospheric turbulence, which significantly increases the bit error rate of free-space optical communication. If the precise prediction of power fluctuations can be achieved, it will be of great benefit for improving communication efficiency. To achieve this goal, this paper proposes a novel Time Series Long Short-Term Memory Fully Connected Processing Network (TSLSTMFCPN), which consists of two long short-term memory (LSTM) network layers and a fully connected layer, for predicting the power fluctuations of laser beams caused by atmospheric turbulence. The experimental results show that the mean absolute percentage error of the TSLSTMFCPN in predicting laser power fluctuations is only 1.2%. This result indicates that this model can accurately predict the laser power fluctuations caused by atmospheric turbulence. Our results are expected to be applied in free-space optical communication systems and imaging laser radar system.

Keywords: atmosphere turbulence; laser propagation; power prediction; long short-term memory (LSTM) network

Citation: Wan, Z.; Zhu, J.; Huang, C.; He, Z.; Zeng, J.; Chen, F.; Yu, C.; Li, Y.; Chen, H.; Zhang, Y.; et al. Prediction of power fluctuations of Gaussian beams after transmission through turbulent atmosphere. *Photonics* **2024**, *11*, 1108. https://doi.org/10.3390/photonics11121108

Received: 30 September 2024
Revised: 9 November 2024
Accepted: 11 November 2024
Published: 22 November 2024

1. Introduction

Due to the combined effects of various natural factors, such as pressure differences, temperature changes, wind shear, and more, a unique optical turbulence field is formed at the Earth's surface. When a light beam traverses this turbulence field, refraction and scattering occur due to the uneven distribution of the air refractive index, a phenomenon known as the atmospheric turbulence effect [1–3]. This effect significantly disrupts the photoelectric systems within the Earth's atmosphere, including laser communication systems, target detection equipment, and astronomical observation devices [4–9]. Specifically, in applications like remote sensing and long-distance imaging, atmospheric turbulence significantly degrades image quality, resulting in optical distortions and blurring [10,11]. Especially in the field of free-space optical communication, the random fluctuations in laser power induced by atmospheric turbulence directly elevate the bit error rate during the communication process, adversely affecting the reliability and efficiency of information transmission [12,13]. In situations where the impact of atmospheric turbulence on laser beam propagation cannot be completely avoided, the ability to accurately predict the fluctuations in laser power caused by atmospheric turbulence, even if only for short-

term fluctuations, would be of paramount importance for enhancing the stability and performance of free-space optical communication. For instance, if the range of power fluctuations can be accurately predicted, a precise evaluation of the error rate of free-space optical communication systems can be obtained. As is well known, the intensity of atmospheric turbulence is closely dependent on meteorological conditions, and this intensity directly determines the amplitude of power fluctuations in laser beams propagated through the atmosphere [14–16]. Given the relatively straightforward and feasible acquisition of meteorological data, investigating how to utilize these routine meteorological data to predict laser power fluctuations undoubtedly represents a research topic of great significance.

Apart from being influenced by meteorological data such as temperature, pressure, and humidity, the effect of atmospheric turbulence on laser beams is also significantly constrained by the wavelength and mode of the beams themselves [17–19]. As a result, a complex nonlinear relationship exists between fluctuations in laser power and meteorological conditions, which renders research on optical turbulence based on traditional physical models often unsatisfactory [20–23]. In the past few years, the rapid development of artificial intelligence and computing power has enabled deep learning to be widely applied in various fields. For instance, in 2016, Wang et al. pioneered the introduction of artificial neural networks at the Mauna Kea Observatories, conducting a month-long study on estimating atmospheric optical turbulence intensity, thereby opening a new chapter in this field [24]. Subsequently, in 2017, Lv et al. collected three key meteorological parameters—temperature, wind speed, and relative humidity—over four consecutive days in Sanya, and leveraged a Back-Propagation Neural Network (BPNN) to accurately estimate the atmospheric refractive index structure constant (e.g., C_n^2) [25]. Following this, Chen et al. further innovated by integrating neural networks with a Genetic Algorithm (GA) to optimize and upgrade the neural network models of Wang and Lv, ultimately achieving effective prediction of C_n^2 using actual meteorological observation data from the northwest plateau of China [26]. These research achievements demonstrate the remarkable feasibility and potential of deep learning methods in establishing complex nonlinear relationships between meteorological data and atmospheric turbulence intensity. Based on this, to achieve the accurate prediction of power fluctuations in laser beams propagating through a turbulent atmosphere with the aid of meteorological parameters, this study designs and constructs a model named the Time Series Long Short-Term Memory Fully Connected Processing Network (TSLSTMFCPN). This model, meticulously constructed with two LSTM layers and a fully connected layer, aims to deeply mine information from measured meteorological data, thereby enabling the precise prediction of power fluctuations in laser beams propagating through a turbulent atmosphere.

2. Data Acquisition and Processing

Data represent the foundation of deep learning, and data preprocessing is an indispensable prerequisite step in building efficient machine learning models. In order to train a model with excellent performance, the data used must fully reflect the essential characteristics of the problem to be modeled. Meanwhile, the testing set should have a certain degree of representative consistency with the training set to ensure the model's generalization ability on unseen data. The first step of our research was to obtain adequate and appropriate data to form data sets for training, validating and testing the neural network model proposed.

To initially validate the concept, a turbulence pool simulating a turbulent atmosphere was constructed in the laboratory, in which some meteorological parameters can be artificially controlled. A hot plate in the turbulence pool is used to heat the air above it so that a simulated atmospheric turbulence layer is formed above the hot plate, the intensity of which can be effectively controlled by adjusting the temperature of the hot plate. The air

in the turbulence pool can be heated up to temperatures well above the atmospheric temperature of natural environments so that a wider range of turbulence intensity can be obtained. Other meteorological data that were collected during the turbulence pool experiment included ambient illuminance, wind speed, and atmospheric pressure, which remained nearly constant during the experimental process. The setup of the turbulence pool experiment is illustrated schematically in Figure 1. A laser beam is expanded and then travels through the simulated atmospheric turbulence in the turbulence pool. An optical power meter and meteorological detection sensors are connected to a computer to measure and record the output laser power and meteorological data in the turbulence pool simultaneously at fixed intervals (time steps). The meteorological data collected include temperature, atmospheric pressure, humidity, wind speed, and illuminance along the laser transmission path. The laser employed is a helium–neon laser, which outputs a Gaussian beam in the fundamental mode. Note that the laser beam is simply expanded without any further modulation of the wave-front phase or polarization, so the beam propagating through the turbulence pool is a Gaussian beam in the fundamental mode.

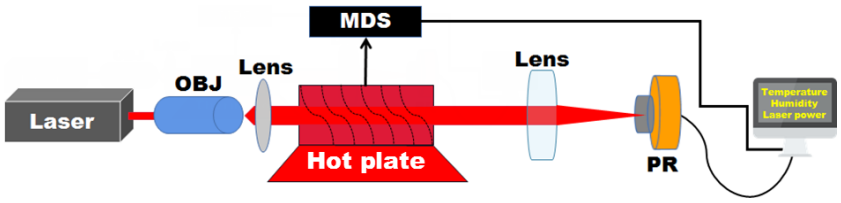

Figure 1. Diagram of simulated turbulence experimental setup. OBJ: objective; MDS: meteorological detection sensors; PR: photocurrent receiver.

As described above, the atmospheric turbulence in this experiment was simulated in a laboratory setting, and its intensity actually depends merely on the temperature of the hot plate, which directly determines the air temperature along the laser propagation path. In addition, the measured meteorological data showed that the ambient illumination, air pressure, and wind speed in the turbulent pool remained almost constant, but the humidity of the air along the propagation path of the laser beam was significantly different at different hot plate temperatures. The temporal fluctuations of the output laser power at different air temperatures are plotted in Figure 2. Comparing the power fluctuations at different air temperatures, it can be clearly observed that the amplitude of the laser's power fluctuation increases significantly with an increase in the temperature of the air in the laser's transmission path. This reflects that with the elevation of the hot plate temperature, the intensity of the turbulence above the hot plate is remarkably strengthened due to deeper air convection.

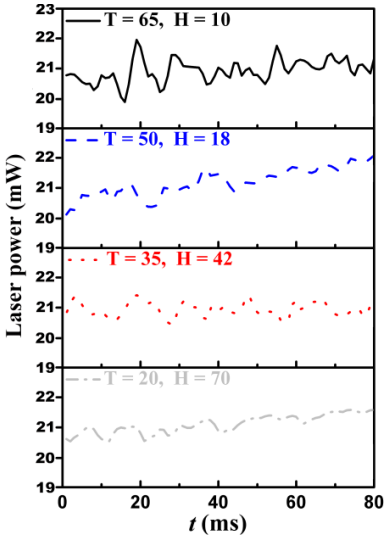

Figure 2. Fluctuations in laser power at different temperatures. T: air temperature of the turbulence pool; H: air humidity of the turbulence pool.

The ultimate goal of the proposed approach is that it can be used in real-world applications, especially in outdoor applications, so the data acquisition experiment was then moved from the laboratory to outdoors. The outdoor data acquisition setup was similar to that in the laboratory. As shown in Figure 3, the helium–neon laser was placed on the fifth floor of the Science and Technology Building of Minnan Normal University, and the data acquisition instrument was installed on the fifth floor of the Dali Building. A miniature meteorological station was set up in the transmission path of the laser for the simultaneous acquisition of meteorological data, including atmospheric temperature, atmospheric pressure, atmospheric humidity, wind speed, and ambient illuminance, at fixed intervals. The experiment was conducted at night to minimize the impact of ambient light on the measurements.

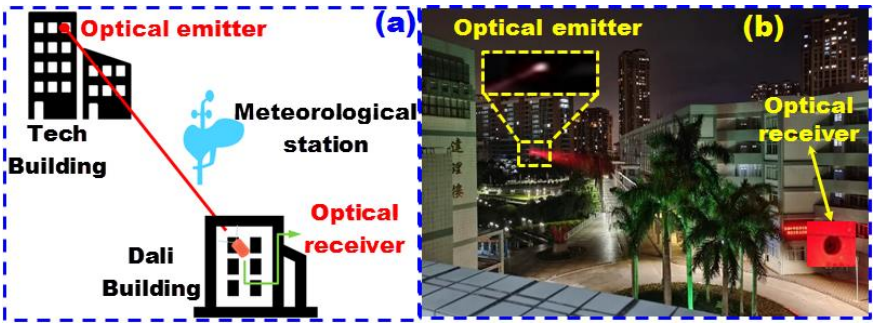

Figure 3. The data acquisition setup in the outdoor experiments. (**a**) A schematic diagram of the experimental optical path. (**b**) An actual photograph of the experimental optical path. The length of the optical link is 200 m, and the beam waist radius of the emitted Gaussian beam is 5 mm.

Before being used for the training of the neural network model and the prediction of laser power fluctuation, all the collected data were first pre-processed. A sliding window algorithm was used to segment the laser power data and meteorological data into groups, each of which contained the laser power and the meteorological parameters collected in one acquisition step. Taking each group of the above data as the input and the laser power collected at the next acquisition step as the output, an input–output data pair was formed, through which a data set was finally established. The data being input into the neural network model were actually a two-dimensional array, each row of which contained the results of one data acquisition step (one time step) and whose columns indicated the parameters being acquired (number of features). The inputs of batch size, time step length, and output dimension were also required for the LSTM model, which are specified in this study as 32, 32 and 8, respectively. These values signify that the model takes 32 data groups coming from 32 consecutive time steps into a batch as a single input, and then predicts the laser power of the 8 time steps following those 32 time steps. The data segmentation and prediction method are illustrated in Figure 4. In addition, the numerical ranges of different features in a data set may vary significantly, which may lead the neural network model to exhibit bias towards features with larger numerical ranges during training, thereby degrading the model's performance. Normalization of the data in the data set is a typical solution to this problem. In this study, a min–max normalization method was utilized, which computes the minimum and maximum values for each feature and then maps the value of each data point to the interval [0,1], ensuring that the model treats all features equally during training. The min–max normalization method is expressed as follows:

$$\hat{x} = \frac{x - x_{\min}}{x_{\max} - x_{\min}} \tag{1}$$

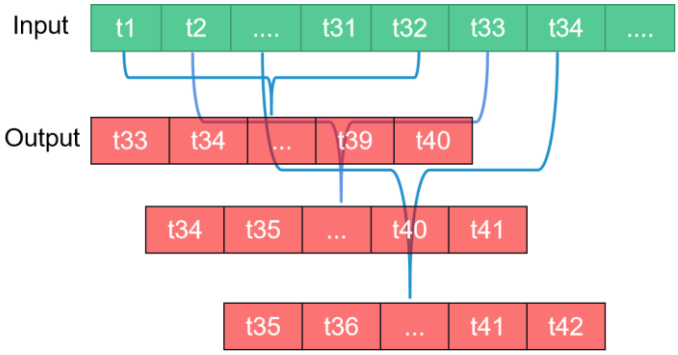

Figure 4. Sliding window algorithm diagram.

After completing the data preprocessing, the data set used for training was inputted into the TSLSTMFCPN. After the training was completed, the TSLSTMFCPN was utilized to predict the laser power fluctuation.

3. Construction of the TSLSTMFCPN

Predicting laser power fluctuation caused by turbulence is essentially a process of processing time-series data, which utilizes memory mechanisms and prior information to effectively process sequence data of arbitrary length. The most commonly used network architecture for time-series data prediction is the Recurrent Neural Network (RNN), as shown in Figure 5a. The chained structure of RNNs comprises repeating modules, which enables them to retain and utilize prior information. For instance, let x_t represent the input value at time t, and h_{t-1} be the hidden state obtained after learning from the previous moment. The prediction of x_{t+1} at the next moment depends on the value of h_t at the current moment. The updating of the previous layer involves multiple arithmetic product operations, which usually leads to gradient vanishing (gradients approaching zero) or gradient explosion (gradients growing exponentially) in the learning process of the RNN. To address this issue, an LSTM (Long Short-Term Memory) architecture was adopted in this study, which is shown in Figure 5b. The fundamental structure of an LSTM unit comprises a forget gate, an input gate, and an output gate. By utilizing these gates to either remove information from or add information to the cell state, it can mitigate the issues of vanishing or exploding gradients that arise in RNNs. An LSTM unit updates six parameters during each iteration, with the specific algorithm detailed as follows:

Step 1: The forget gate decides what information should be discarded or forgotten by the cell state. This is decided based on the previous hidden state $\overrightarrow{h_{t-1}}$, the current input $\overrightarrow{x_t}$, the learnable weights W_{xf}, W_{hf}, and the biases $\overrightarrow{b_f}$, as expressed by

$$\overrightarrow{f_t} = \sigma(W_{xf}\overrightarrow{x_t} + W_{hf}\overrightarrow{h_{t-1}} + \overrightarrow{b_f}) \tag{2}$$

The σ curve maps values between 0 and 1, in which 1 represents the prior information being completely retained, and 0 represents the prior information being completely forgotten.

$$\sigma(x) = \frac{1}{1 + \exp(-x)} \tag{3}$$

Step 2: The input gate determines what information is to be stored in the cell unit, which involves two main components. The first one utilizes the σ function to decide

which data need to be updated, and the second one employs the tanh function to create a temporary cell state $\overline{C_t}$ for the new candidate values.

$$\vec{i}_t = \sigma\left(W_{xi}\vec{x}_t + W_{hi}\overrightarrow{h_{t-1}} + \vec{b}_i\right) \tag{4}$$

$$\overline{\boldsymbol{C}_t} = \tanh(W_{xc}\vec{x}_t + W_{hc}\overrightarrow{h_{t-1}} + \vec{b}_c) \tag{5}$$

Once the memories that need to be forgotten and those that need to be added are determined, the old cell state $\overline{C_{t-1}}$ can be updated to the new cell state $\overline{C_t}$.

Step 3: The updated cell state $\overline{C_t}$ is combined with the output gate $\vec{o}_t$ to calculate the new hidden state.

$$\vec{o}_t = \sigma\left(W_{ox}\vec{x}_t + W_{ho}\overrightarrow{h_{t-1}} + \vec{b}_o\right) \tag{6}$$

$$\vec{h}_t = \vec{o}_t \otimes \tanh\left(\overline{C_t}\right) \tag{7}$$

In Equations (6) and (7), the operator $\otimes$ represents an element-wise product, W_{ox} and W_{ho} are the weight matrices, and $\vec{b}_o$ is the bias vector.

In order to improve the performance of the entire model, two LSTM layers are stacked and followed by a fully connected layer to output multiple predictions in chronological order. As shown in Figure 6, the Time Series Long Short-Term Memory Fully Connected Processing Network (TSLSTMFCPN) architecture consists of two LSTM layers and a fully connected layer. In each time step of data acquisition, five meteorological parameters, including temperature, humidity, wind speed, atmospheric pressure, and ambient illuminance, are measured and stored simultaneously. The data from 32 consecutive time steps are grouped into a batch as a single input for the model. Then, the TSLSTMFCPN outputs eight values of laser power predictions for the 8 time steps that just followed the previous 32 time steps of the input.

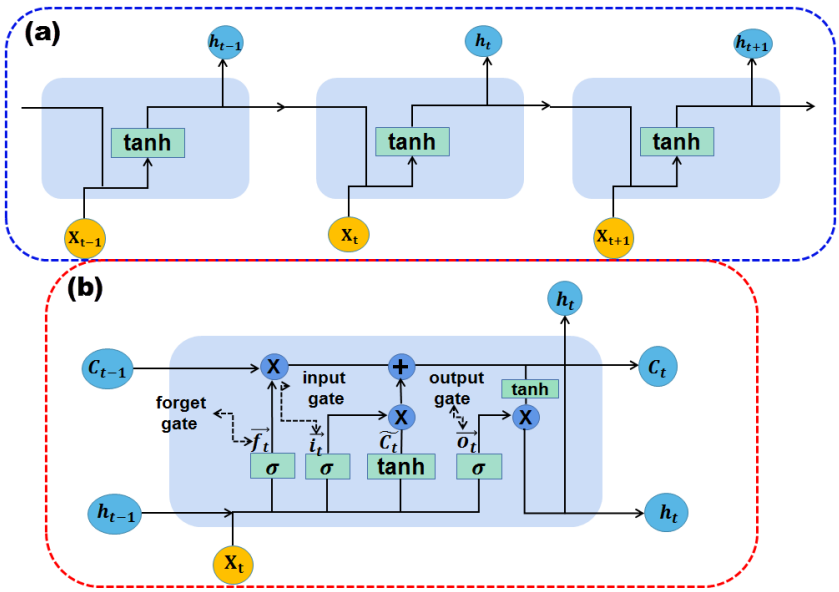

Figure 5. (**a**) Schematic of RNN chain structure; (**b**) schematic of LSTM unit structure.

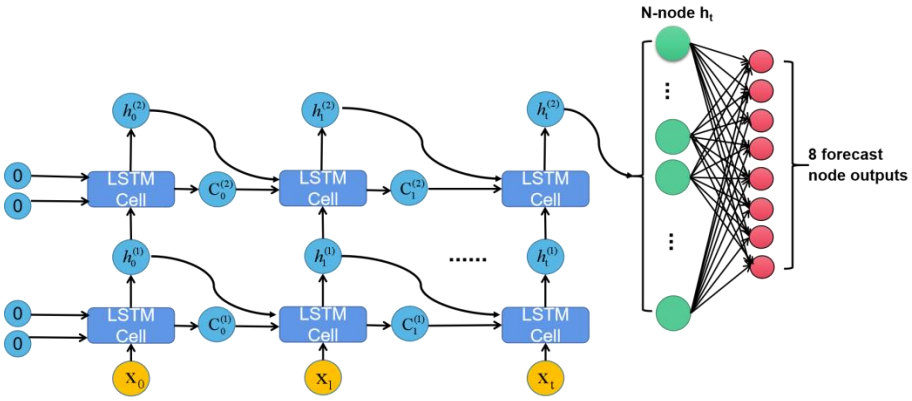

Figure 6. Schematic of TSLSTMFCPN architecture.

For the training of the TSLSTMFCPN, a Root-Mean-Square Error (RMSE) function is used as the loss function, which is defined by

$$\mathrm{RMSE} = \sqrt{\frac{1}{N}\sum_{i=1}^{N}\left|y_i - \overline{y_i}\right|^2} \tag{8}$$

In Equation (8), y_i represents the measured value at time i, and $\overline{y_i}$ represents the predicted value at time i. In order to minimize the training error while avoiding the occurrence of local minimum points, an Adam optimizer was utilized, which has an adaptive learning rate for back-propagation. Meanwhile, normalization was applied to the data of laser power and meteorological parameters for data preprocessing, and L2 regularization was applied to the TSLSTMFCPN to reduce overfitting. Figure 7 illustrates the prediction error rates of the TSLSTMFCPN after being trained for different rounds of training epoch (training iteration), in which (a) was obtained using the data collected in the turbulence pool experiment and (b) in the outdoor experiment. From both curves, it can be seen clearly that the model's prediction error decreases with an increase in training epoch, and remains constant as the training epoch reaches about 30 rounds.

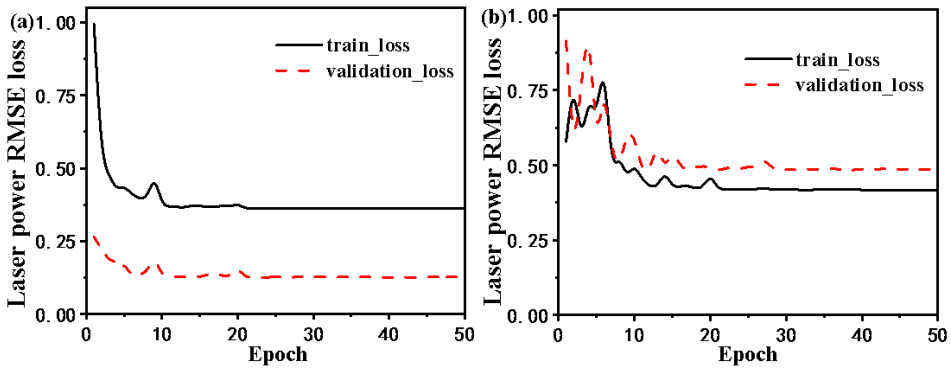

Figure 7. Prediction error rate of TSLSTMFCPN vs. rounds of training epoch (**a**) using data collected in turbulence pool experiment and (**b**) using data collected in outdoor experiment.

4. Prediction Results and Discussion

The performance of the TSLSTMFCPN in the prediction of laser power fluctuation caused by atmospheric turbulence was initially inspected using the data collected in the turbulence pool experiment. The training epoch and the initial learning rate were set to 50 and 0.01, respectively. A staircase learning rate decaying strategy was adopted, in which the learning rate is reduced to 0.1 times its previous value in each training epoch, and the beta parameter in the Adam optimizer was set to the default value (0.9, 0.999). The TSLSTMFCPN employs the Root-Mean-Square Error (RMSE) as the loss function and

adopts Adam as the optimization strategy. The Adam optimizer boasts computational efficiency, low memory requirements, and applicability to large-scale data and parameters. Additionally, its adaptive learning rate adjustment mechanism can significantly enhance training efficiency. This aids us in rapidly converging to optimal network parameters, thereby improving the network's prediction accuracy. Moreover, two benchmarks, the mean absolute error (MAE) and the mean absolute percentage error (MAPE), were used to evaluate the performance of the TSLSTMFCPN in predicting the laser power fluctuation caused by atmospheric turbulence, which give a quantitative indication of the difference between the predicted and measured values. The MAE and MAPE are defined as

$$\mathrm{MAE} = \frac{1}{N}\sum_{i=1}^{N}\left|y_i - \overline{y_i}\right|^2 \tag{9}$$

and

$$\mathrm{MAPE} = \frac{100\%}{N}\sum_{i=1}^{N}\frac{\left|y_i - \overline{y_i}\right|^2}{y_i}, \tag{10}$$

where y_i represents the measured value at time i, and $\overline{y_i}$ represents the predicted value at time i. If the predicted value given by a neural network model perfectly matches the measured value, the MAE equals 0, indicating an ideal model capable of accurate prediction. The MAPE is the mean absolute error obtained by the normalized error of each point, which can effectively mitigate the effect of individual outliers on the overall absolute error. A lower percentage value of the MAPE signifies higher prediction accuracy of a neural network model.

As mentioned previously, the laser power and the meteorological parameters, including atmospheric temperature, atmospheric pressure, humidity, wind speed, and ambient illuminance, were acquired simultaneously in the turbulence pool experiment. The data collected by the experiment were divided into a training set, a verification set, and a test set according to proportions of 85%, 10%, and 5%. The data of laser power and meteorological parameters were used as the input and the laser power as the output for the training of the TSLSTMFCPN. Once the trained model was fed with new input data, multiple predicted laser power values for the subsequent time steps were output. Figure 8a illustrates a comparison between the measured laser power values and those predicted by the TSLSTMFCPN using the data obtained in the turbulence pool experiment. It can be seen that the profile of the laser power values predicted by the model matches well with the measured one. The MAE and MAPE were calculated as 0.0598 milliwatt and 0.3%, respectively. These results demonstrate that the TSLSTMFCPN is able to accurately predict laser power fluctuations caused by atmospheric turbulence. Note that the measured ambient illuminance and wind speed remained almost constant in the turbulence pool experiment. In other words, these two meteorological parameters do not contribute to the laser power fluctuation. Then, they were removed from the input data for the network training and prediction, that is, the new input data included laser power, temperature, humidity, and pressure, and the results of the prediction are illustrated in Figure 8b. By comparing Figure 8a and Figure 8b, it can be observed that the prediction accuracy of the TSLSTMFCPN is further improved when the data unrelated to the laser power fluctuation are excluded from the input data for network training and prediction, in which the MAE decreases from 0.0598 milliwatt to 0.0583 milliwatt.

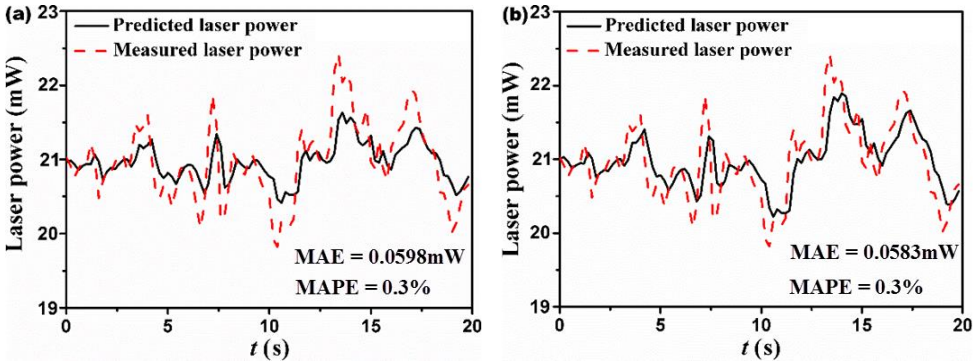

Figure 8. Laser power measured and predicted by TSLSTMFCPN using data obtained in turbulence pool experiment (**a**) using all collected meteorological parameters as model input and (**b**) using meteorological parameters of temperature and humidity only as model input.

Turbulence in outdoor natural environments is far more complex than the artificial turbulence in a turbulence pool, and thus, the laser power fluctuation they cause is far more difficult to predict. To examine the performance of the TSLSTMFCPN in the prediction of laser power fluctuations in natural environments, data collected in the outdoor experiment were used for the neural network model training and laser power prediction. The outdoor meteorological parameters collected included atmospheric temperature, atmospheric pressure, humidity, ambient illuminance, wind speed, and wind direction. These meteorological data and simultaneously collected laser power data were also preprocessed and prepared according to the procedure described in Section 2, and then used to train the TSLSTMFCPN. Once the model training was complete, new data were fed to the model to produce predictions of the laser power for subsequent time steps. The prediction results are shown in Figure 9a along with the measured laser power. Comparing the predicted values with the measured values, it could be concluded that the trained TSLSTMFCPN is capable of making accurate predictions of future laser power fluctuations based on the available laser power data and meteorological data. An MAE value of 0.0121 milliwatt and an MAPE of 1.3% were achieved. It was also observed from the collected outdoor meteorological data that two parameters of atmospheric pressure and ambient illuminance varied little in their values. After the data for these two parameters were excluded from the input data, the training of the model and the prediction of the laser power were performed again, and the results obtained are presented in Figure 9b. Compared with the prediction results shown in Figure 9a, the accuracy of the prediction was improved to a certain extent after this operation, whereby the MAE dropped from 0.0121 milliwatt to 0.0111 milliwatt and the MAPE from 1.3% to 1.2%.

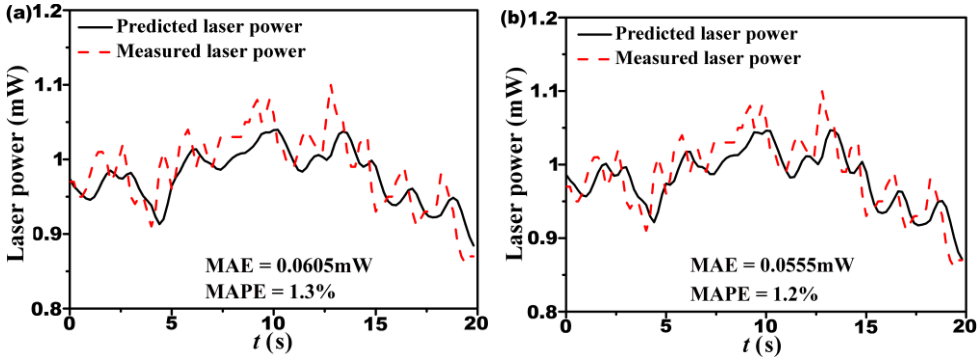

Figure 9. Laser power measured and predicted by TSLSTMFCPN using data obtained in outdoor experiment (**a**) using all collected meteorological parameters as model input and (**b**) using meteorological parameters excluding atmospheric pressure and ambient illuminance as model input.

5. Conclusions

A novel Time Series Long Short-Term Memory Fully Connected Processing Network (TSLSTMFCPN) is proposed to predict future laser power fluctuations caused by atmospheric turbulence based on measured laser power and meteorological parameters. This neural network model is composed of two long short-term memory (LSTM) network layers and a fully connected layer. The power of a laser beam traveling through atmospheric turbulence and some meteorological parameters were collected simultaneously in time steps to form time-series data, which serve as the input to the model, and the laser power of the subsequent time steps was the output for model training. We found that the successfully trained TSLSTMFCPN is able to predict future laser power fluctuations based on current measurements of laser power and meteorological parameters. The experimental results indicate that a high accuracy with a mean absolute percentage error as low as 1.2% in prediction was achieved by the TSLSTMFCPN. The results presented in this paper hold promising application prospects in various fields, including free-space optical communication and imaging laser radar system.

Author Contributions: Conceptualization, Z.W. and H.L.; methodology, H.L., Z.H. and J.Z. (Jun Zeng); software, Z.W., C.H., F.C. and C.Y.; validation, Y.L., H.C. and Y.Z.; investigation, Z.W. and J.Z. (Jiayi Zhu); writing—original draft preparation, Z.W. and J.Z. (Jiayi Zhu); writing—review and editing, H.L. and J.P. All authors have read and agreed to the published version of the manuscript.

Funding: This project was supported by the National Natural Science Foundation of China (NSFC), grant number 12174173. This research was funded by the Natural Science Foundation of Fujian province, grant numbers 2022H0023, 2022J02047, ZZ2023J20, and MSPY2022010; the Industry-University-Research Collaboration Foundation of Fujian Province, grant numbers 2024H6014 and 2022G02006; and the Dongguan Introduction Program of Leading Innovative and Entrepreneurial Talents (China), grant number 201927879.

Data Availability Statement: The original data has not been used to create an additional dataset. For any inquiries regarding the research data used, please contact the corresponding author.

Conflicts of Interest: The authors declare no conflicts of interest.

References

1. Wyngaard, J.C. Atmospheric turbulence. *Annu. Rev. Fluid Mech.* **1992**, *24*, 205–234.
2. Moser, R.D.; Haering, S.W.; Yalla, G.R. Statistical properties of subgrid-scale turbulence models. *Annu. Rev. Fluid Mech.* **2021**, *53*, 255–286.
3. Shapiro, C.R.; Starke, G.M.; Gayme, D.F. Turbulence and control of wind farms. *Annu. Rev. Control Robot. Auton. Syst.* **2022**, *5*, 579–602.
4. Raj, A.A.B.; Krishnan, P.; Darusalam, U.; Kaddoum, G.; Ghassemlooy, Z.; Abadi, M.M.; Majumdar, A.K.; Ijaz, M. A Review–Unguided Optical Communications: Developments, Technology Evolution, and Challenges. *Electronics* **2023**, *12*, 1922.
5. Lukin, V.P.; Antoshkin, L.V.; Bolbasova, L.A.; Botygina, N.N.; Emaleev, O.N.; Kanev, F.Y.; Konyaev, P.A.; Kopylov, E.A.; Lavrinov, V.V.; Lavrinova, L.N.; et al. The history of the development and genesis of works on adaptive optics at the Institute of atmospheric optics. *Atmos. Ocean. Opt.* **2020**, *33*, 85–103.
6. Xue, T.; Lin, D.; He, J.-P. Research status and application prospects of astrophotonics. *Chin. Astron. Astrophys.* **2023**, *47*, 54–90.
7. Abdulwahid, M.M.; Kurnaz, S.; Türkben, A.K.; Hayal, M.R.; Elsayed, E.E.; Juraev, D.A. Inter-satellite optical wireless communication (Is-OWC) trends: A review, challenges and opportunities. *Eng. Appl.* **2024**, *3*, 1–15.
8. Li, R.; Lin, B.; Liu, Y.; Dong, M.; Zhao, S. A survey on laser space network: Terminals, links, and architectures. *IEEE Access* **2022**, *10*, 34815–34834.
9. Brydegaard, M.; Svanberg, S. Photonic monitoring of atmospheric and aquatic fauna. *Laser Photonics Rev.* **2018**, *12*, 1800135.
10. Su, C.; Wu, X.; Guo, Y.; Zhang, S.; Wang, Z.; Shi, D. Atmospheric turbulence degraded image restoration using a modified dilated convolutional network. *IET Image Process.* **2022**, *16*, 3507–3517.
11. Chen, G.; Gao, Z.; Wang, Q.; Luo, Q. Blind de-convolution of images degraded by atmospheric turbulence. *Appl. Soft Comput.* **2020**, *89*, 106131.
12. Nistazakis, H.E.; Tsiftsis, T.A.; Tombras, G.S. Performance analysis of free-space optical communication systems over atmospheric turbulence channels. *IET Commun.* **2009**, *3*, 1402–1409.
13. Khalighi, M.A.; Uysal, M. Survey on free space optical communication: A communication theory perspective. *IEEE Commun. Surv. Tutor.* **2014**, *16*, 2231–2258.
14. Arockia Bazil Raj, A.; Selvi, J.A.V.; Raghavan, S. Real-time measurement of meteorological parameters for estimating low-altitude atmospheric turbulence strength (C_n^2). *IET Sci. Meas. Technol.* **2014**, *8*, 459–469.

15. Trini Castelli, S.; Bisignano, A.; Donateo, A.; Landi, T.C.; Martano, P.; Malguzzi, P. Evaluation of the turbulence parametrization in the MOLOCH meteorological model. *Q. J. R. Meteorol. Soc.* **2020**, *146*, 124–140.
16. Ayet, A.; Chapron, B. The dynamical coupling of wind-waves and atmospheric turbulence: A review of theoretical and phenomenological models. *Bound. Layer Meteorol.* **2022**, *183*, 1–33.
17. Ji, X.; Deng, J. Effect of spherical aberration on scintillations of Gaussian beams in atmospheric turbulence. *Phys. Lett. A* **2014**, *378*, 2729–2735.
18. Cox, M.A.; Mphuthi, N.; Nape, I.; Mashaba, N.; Cheng, L.; Forbes, A. Structured light in turbulence. *IEEE J. Sel. Top. Quantum Electron.* **2020**, *27*, 1–21.
19. Yu, X.; Tu, J.; Wang, X.; Zhang, L.; Deng, D. Statistical properties of a controllable rotating elliptical Gaussian Schell-model vortex optical coherence lattice. *Opt. Commun.* **2021**, *499*, 127276.
20. Sadot, D.; Kopeika, N.S. Forecasting optical turbulence strength on the basis of macroscale meteorology and aerosols: Models and validation. *Opt. Eng*. **1992**, *31*, 200–212.
21. Andrews, L.C.; Phillips, R.L.; Hopen, C.Y.; Al-Habash, M.A. Theory of optical scintillation. *J. Opt. Soc. Am. A* **1999**, *16*, 1417–1429.
22. Dordová, L.; Wilfert, O. Calculation and comparison of turbulence attenuation by different methods. *Radioengineering* **2010**, *19*, 162–167.
23. Li, Y.; Zhu, W.; Wu, X.; Rao, R. Equivalent refractive-index structure constant of non-Kolmogorov turbulence. *Opt. Express* **2015**, *23*, 23004–23012.
24. Wang, Y.; Sukanta, B.S. Using an artificial neural network approach to estimate surface-layer optical turbulence at Mauna Loa, Hawaii. *Opt. Lett.* **2016**, *41*, 2334–2337.
25. Lü, J.; Zhu, W.Y.; Cai, J.; Qing, C. Comparison of two approaches for estimating atmospheric optical turbulence intensity near sea. *Acta Opt. Sin.* **2017**, *37*, 501001.
26. Chen, X.W.; Zhu, W.Y.; Qian, X.M.; Luo, T.; Sun, G.; Liu, Q.; Li, X.B.; Weng, N.Q. Estimation of surface layer optical turbulence using artificial neural network. *Acta Opt. Sin.* **2020**, *40*, 15–21.